DOES THE URBANIZATION OF AGRICULTURAL LAND LEAD TO MORE OR LESS EVAPOTRANSPIRATION?

by

Curtis Ryan Crandall

A thesis

submitted in partial fulfillment

of the requirements for the degree of

Master of Science in Hydrologic Sciences

Boise State University

August 2019

BOISE STATE UNIVERSITY GRADUATE COLLEGE

DEFENSE COMMITTEE AND FINAL READING APPROVALS

of the thesis submitted by

Curtis Ryan Crandall

Thesis Title: Does The Urbanization of Agricultural Land Lead to More or Less Evapotranspiration?

Date of Final Oral Examination: 16 May 2019

The following individuals read and discussed the thesis submitted by student Curtis Ryan Crandall, and they evaluated his presentation and response to questions during the final oral examination. They found that the student passed the final oral examination.

Shawn Benner, Ph.D.	Chair, Supervisory Committee
Alejandro N. Flores, Ph.D.	Member, Supervisory Committee
Jodi Brandt, Ph.D.	Member, Supervisory Committee
Kendra E. Kaiser, Ph.D.	Member, Supervisory Committee

The final reading approval of the thesis was granted by Shawn Benner, Ph.D., Chair of the Supervisory Committee. The thesis was approved by the Graduate College.

DEDICATION

This thesis is dedicated to my wife, Kallie, and our twin boys Charlie and Carter.

ACKNOWLEDGEMENTS

Thank you to my academic adviser for giving me the opportunity to work on this project and guidance during the research process. I also want to thank my excellent committee who kept me on track until the end.

ABSTRACT

Agricultural areas within the western U.S. are undergoing rapid urbanization due to population growth. Urban expansion often forces the conversion of adjacent agricultural areas altering the landscape vegetation and associated water consumption through evapotranspiration (ET). The associated difference in ET may alter the landscape water demand complicating water resource management. To investigate these differences, we calculated the agricultural and urban seasonal ET rates in a semiarid watershed currently undergoing large population growth and rapid urbanization. We used high resolution satellite imagery with a GIS computer model to generate basin-wide ET estimates over a 204-day irrigation season. Six land type samples (three agriculture and three urban) were analyzed to compare individual spatial and temporal variations of ET throughout the irrigation season. The agricultural areas exhibited more fluctuation in seasonality and magnitude of ET than the urban areas throughout the irrigation season. We found the average ET (mm $acre^{-1}$) of the total urban land was 20% less than the total agricultural land within the study area. This is higher than expected due to the urban areas having much less average vegetation per acre. Within the land type samples, some urban landscapes show upwards of 20% more ET (mm $acre^{-1}$) than adjacent agricultural land. These results indicate the difference in total ET between urban and agricultural areas is contingent on the specific vegetation phenology. As urbanization and land development continues, we suggest future needs for irrigation water incorporate current and projected landscape vegetation type, seasonal phenology, and spatial coverage.

TABLE OF CONTENTS

LIST OF TABLES

LIST OF FIGURES

LIST OF ABBREVIATIONS

m	meter
mm	mm
af	acre feet
ft	foot
GIS	Geographical Information Systems
DCMI	Domestic Commercial Municipal Industrial
ET	Evapotranspiration
ET_a	Actual Evapotranspiration
ET_{rs}	Tall Grass Reference Evapotranspiration
K_c	Crop Coefficient
Kc_{evi}	Crop Coefficient from EVI
VI	Vegetation Index
EVI	Enhanced Vegetation Index
NDVI	Normalized Difference Vegetation Index
IDWR	Idaho Department of Water Resources
IDEQ	Idaho Department of Environmental Quality
NHD	National Hydrography Dataset
CI	Confidence Interval

INTRODUCTION

Urbanization impacts the annual water demand and energy balance of a landscape due to the large changes in spatial coverage and type of vegetation (Qiu et al., 2013; Stow et al., 2003). Population growth has accelerated the rate of urbanization across the U.S. over the last half century (Ehrlich and Ehrlich, 1990). One of the main ways land use cover change affects the regional water balance is through changes in evapotranspiration (ET). ET is the combination of evaporation and transpiration and is controlled by temperature, albedo, water availability, wind, humidity, vegetation type and extent. Vegetation type and coverage is a significant driver of differences in ET between urban and agricultural landscapes (Taha, 1997; Qiu et al., 2013).

Regional and local urban hydrologic information is essential for the continued growth and prosperity of any given city. City planners and decision makers need to know how water consumption and availability will change to ensure future water needs are met and risks are mitigated (Niemczynowicz, 1999). Without understanding the effects of urbanization, cities may find their water needs outgrow their available supply (Barnett, Adam, and Lettenmaier, 2005).

ET is often overlooked or over simplified, in part due to the inherent complexity and difficulty in acquiring direct ET measurements (Howell, Schneider, and Jensen, 1991; Valayamkunnath, Sridhar, Zhao, and Allen, 2018). ET may also be an understudied variable within a local urban water balance if the region is not currently under a large water supply stress. While it may be self-evident that the ET of a developed area like a

parking lot is drastically lower than an alfalfa field, it is less obvious when the urbanized area includes large green spaces common in suburban neighborhoods (Grimmond and Oke, 1999) (Figure 1).

ET is measured and calculated with a variety of methods, including both field instrumentation and remote sensing products. Directly measuring ET is typically very expensive, requires a high level of maintenance and extensibility is spatially limited (Alfieri, Kustas, and Anderson, 2018). Additionally, urban microclimates create high variability, which degrades the spatial accuracy of ET estimates when point measurements are extrapolated (Li and Heap, 2014; Allen, Pereira, Howell, and Jensen, 2011; Grimmond and Oke, 1999; DiGiovanni-White, Montalto, and Gaffin, 2018; Templeton et al, 2018).

While there are multiple methods and equations to calculate ET (Amatya, Skaggs, and Gregory, 1995; Khoob, 2008), the most widely adapted ET equation is the Penman-Monteith (PM) combination formula (Allen, Jensen, Wright, and Burman, 1989; Allen, Pereira, Raes, and Smith, 1998). This formula calculates a reference ET value using commonly available climate variables and may be combined with a crop coefficient to produce actual ET estimates (ASCE-EWRI, 2005). The now standardized ET equation is widely used in ET models and has shown to produce reliable estimates in semiarid areas when compared with direct instrument measurements (within 5%) (Allen 2002; López-Urrea, de Santa Olalla, Fabeiro, and Moratalla, 2006; Gavilan, Berengena, and Allen, 2007; Allen, Tasumi, and Trezza, 2007).

Remote sensing-based approaches are used often due to the ability to estimate ET over large areas (Glenn, Nagler, and Huete, 2010; Allen et al. 2007; Nouri, Glenn,

Beecham, Chavoshi Boroujeni, Sutton, Alaghmand, and Nagler, 2016; Nagler et al. 2013). Accuracy of remote sensing models are found to be within 10-40% (Allen et al., 2011) of measured ET values. One of the most widely used methods is the Mapping Evapotranspiration at high Resolution with Internalized Calibration (METRIC) method. This model and others like it, utilize the Landsat satellite imagery to model and map a region's annual ET at a 30-meter resolution, producing estimates within 10% of measured values in agricultural fields and rangelands (Allen et al., 2007; Trezza, Allen, and Tasumi, 2013; Paco et al., 2014). However, an urban ET analysis requires a finer spatial and temporal resolution to precisely separate nonpermeable and vegetated surfaces.

Other remote sensing applications utilize vegetation indices to produce ET estimates each pixel of the satellite image. Previous studies have used vegetation index models to accurately model regional ET using a lower resolution MODIS satellite image data set (Nagler et al., 2005; Nouri et al., 2016). These vegetation index methods require less specific band information, which enables the use of a broader range of newer satellites. Although newer satellite programs often have limited available band information, they have much higher spatial and temporal resolutions. These very high-resolution satellite images have been used with ET models to produce precise (within 10% of instrument data) local ET estimates (Nouri, Beecham, Anderson, and Nagler, 2014).

Understanding ET in urban environments is critical for future water resource planning in regions undergoing urbanization that may be susceptible to drought. However, a reliable network of instrumentation throughout an urban environment is

expensive, spatially limited, and prone to biased measurements given urban microclimates. Here we use satellite imagery that features higher spatial and temporal resolution than both Landsat and MODIS to model and estimate changes in ET following urbanization. The higher spatial resolution imagery allows better separation of urban and agricultural landscapes. The higher temporal resolution enables differentiation between agricultural and urban vegetation phenology throughout the irrigation season. The resulting ET estimates are then used to calculate current and future irrigation water demand based under different growth scenarios.

METHODS

Site Description

This study was conducted on the Lower Boise River Basin which is commonly referred to as the Treasure Valley. The Lower Boise River Basin is in the semiarid portion of southwestern Idaho, within the Pacific Northwest of the United States (Figure 2). The total basin area is approximately 1,300 square miles and it receives 11 inches of precipitation annually (Thornton, Thornton, Mayer, Wilhelmi, Wei, Devarakonda, and Cook, 2014). Water demand in the lower basin is met by a complex network of reservoirs, rivers, canals, and drains. This system is largely responsible for sustaining commercial and domestic life in the basin.

The 2015 Idaho Department of Water Resources (IDWR) land classification data for the Treasure Valley shows the divide between urban and agricultural use (semi-irrigated and irrigated, Figure 2). There are 160,000 acres of urban area and 220,000 acres of agriculture. The agricultural land in the lower basin is primarily occupied (more than 70%) by alfalfa, corn, wheat crops (USDA, 2017). The urban area has areas of high and low-density coverages of predominantly turf grass and tree varieties. The basin's annual irrigation water demand through ET is estimated to be between 600,000 and 750,000 acre-feet using a water balance approach (Treasure Valley Water Atlas, 2018).

ET Modeling Methods

We used high resolution satellite imagery and local climate data to model and calculate daily ET (Figure 4). The remote sensing model approach calculates ET at each

pixel by using a reference ET and a crop coefficient (Figure 5). This method provides a robust solution to the more spatially limited alternatives of direct ET measurement.

The high-resolution imagery comes from the Sentinel-2 satellite program. Sentinel-2 is a satellite system supporting Copernicus Land Monitoring studies, including monitoring vegetation, soil, and water cover. The satellites offer 10 m resolution multispectral images with up to a 5-day temporal resolution. A total of 22 cloud free images were used covering the irrigation season from April 4th to October 24th, 2017. Each image was processed to convert from Sentinel Level-2A Top-of-Atmosphere (TOA) reflectance values to Sentinel Level-2C Bottom-of-Atmosphere (BOA) surface reflectance values (Appendix 1). The BOA values are required to run near surface calculations and correct for atmospheric interference. The Enhanced Vegetation Index (EVI) was calculated for each image using the red (RED), blue (BLUE), and near-infrared (NIR) bands (Eq. 1).

$$2.5 \cdot \frac{NIR - RED}{NIR + (6 \cdot RED) - (7.5 \cdot BLUE) + 1} \quad (Eq. 1)$$

To address temporal gaps within the EVI time series, new images were created between satellite image dates. This created daily EVI values for each image to correspond with daily climate values within the model. A minimum of 5 days exists between each image given the timing and pathing of the Sentinel satellites and larger gaps may exist due to interreference from cloud cover. A weighted linear interpolation was used to create each new based on the EVI data between two original Sentinel images (Eq.2)

$$\mathrm{Image_n} = [(\mathrm{Image_1} \cdot \mathrm{W_1}) + (\mathrm{Image_2} \cdot \mathrm{W_2})]; \text{ when } \begin{bmatrix} \mathrm{W_1} = \dfrac{\#\mathrm{Days} - \mathrm{Day}i}{\#\mathrm{Days}} \\ \mathrm{W_2} = \dfrac{\mathrm{Day}i}{\#\mathrm{Days}} \end{bmatrix} \quad (Eq. 2)$$

Where $Image_n$ is the new interpolated EVI image, $Image_1$ is the starting satellite image, $Image_2$ is the ending satellite image, #Days is the total number of days between $Image_1$ and $Image_2$, Day_i is the interpolation day index number, W_1 is the weighted EVI value based on the number of days from $Image_1$, and W_2 is the weighted EVI value based on the number of days from $Image_2$. Interpolating between the EVI images, allowed us to use daily climate variables.

Climate data was acquired from Bureau of Reclamation's AgriMet stations. Each station measures daily climate data variables, including an ASCE tall grass reference ET rate, which is used directly in calculating an actual ET estimate. Three stations were available to use within the study area. They are each located in separate parts of the basin which represent different land cover types including both urban and agriculture (Figure 2). The daily data used within the model is an average of all the stations. Since the stations are in different locations across the study area, using any single station would produce ET calculations biased for that environment. By averaging all available station data, it provides a better representation of climate values across the basin.

Calculating actual ET first requires a reference ET value. This is the ET rate from a reference surface for a specific crop that is not under water stress under current climate conditions. Alfalfa is the most common reference surface used across hydrologic studies, but a short grass reference may also be used. Both variations, described in the FAO-56 formulation (Appendix 2), have been shown to model accurate reference ET estimates (Kite and Droogers, 2000). We used a tall grass reference ET (ETrs) that was standardized from the American Society of Civil Engineers (ASCE) in 2005:

$$ET_{rs} = \frac{0.408 \cdot \Delta \cdot (R_n - G) + \gamma + \frac{1600}{T + 273} \cdot U_2 \cdot (e_s - e_a)}{\Delta + \gamma \cdot (1 + 0.38 \cdot U_2)} \quad (Eq. 3)$$

Where Δ is the slope of the saturation vapor pressure-temperature gradient, R_n is the net solar radiation at the crop surface, G is the soil heat flux density at the crop surface, T is the mean air temperature 2 meters above the crop surface, e_s is the saturated vapor pressure 2 meters above the crop surface, e_a is the actual vapor pressure 2 meters above the crop surface, γ is the psychrometric constant, and U_2 is the wind profile factor.

The type of crop coefficient (Kc), or the value representing a crop type and developmental stage, used in the ET model is a single crop coefficient. The single Kc averages the measurable effects of crop transpiration and soil evaporation into a single term (Allen et al., 1998). Single Kc coefficients used in past evapotranspiration projects were found to produce values within 5% of dual Kc during sensitivity analysis of the two coefficient types (Allen et al., 2005b). A satellite derived vegetation index value can replace a standard crop coefficient to produce an ET estimate based on current crop (Glenn et al., 2010). Remote sensing derived crop coefficients have a strong relationship with directly measured crop coefficients (r^2 = 0.90, Kamble, Kilic, and Hubbard, 2013). This approach results in a unique crop coefficient for each pixel of an image.

The EVI was used to calculate crop coefficients, which are combined with a local reference ET to calculate an actual ET rate (Glenn et al., 2010). Previous applications of these EVI methods resulted in modeled ET values within 2-9% of direct instrument measurements (Nouri et al., 2016). The crop coefficient algorithm used was:

$$Kc_{evi} = 1.48 \cdot (1 - e^{-2.95 \cdot EVI}) - 0.49 \; (Eq. 4)$$

Where Kc_{evi} is the derived pixel crop coefficient, and EVI is the EVI value at each pixel.

The daily observed ET estimates from the AgriMet stations were used to calibrate the model (Eq. 4) using a minimizing gradient search method to provide the best fit.

Linear regressions were used to evaluate the modeled ET versus the observed ET estimates at the Boise and Parma AgriMet stations (Montgomery, Peck, and Vining, 2012).

The daily actual ET (ET_a) estimates are the product of the daily reference ET (ET_{rs}) and a crop coefficient (Kc) (Allen et al., 2005a). We substituted the traditional Kc value from a table with an EVI based crop coefficient (Kc_{evi}) and applied Eq 5 to every pixel of each image:

$$ET_a = ET_{rs} \cdot Kc_{evi} \ (Eq.5)$$

where ET_{rs} is the daily basin averaged reference ET, and ET_a is the actual ET of each pixel.

Modeled ET was validated against ET values calculated at the AgriMet station locations. Each station sits in, or is adjacent to, a uniform crop type, such as turf grass or a corn. Each crop type has a locally derived crop coefficient timing curve (Henggeler Guinan, and Travlos, 2008). These coefficients were combined with a daily reference ET to provide a local ET estimate (Allen et al., 1998; Rick Allen, 2000; Itenfisu, Elliott, Allen, and Walter, 2003; Allen et al., 2005a).

Identification of Unique Land Uses

Total ET and ET per acre was calculated for eight different land use subsets. These include, the 2015 total agriculture and total urban areas for the basin (IDWR, 2009), three agricultural crop types (alfalfa, corn, and wheat) and three urban types (low density, medium density, and high density). The agricultural land use samples were created using the 2017 USDA CropScape data (USDA 2017).

Housing clusters were identified to classify the urban density land use samples. A Maximum Likelihood Classifier (MLC) was used to identify pixel clusters representing houses. The layers consist of approximately 3 to 6 houses per acre for each 9-acre sample area. Sample areas are identified around subdivisions inside metropolitan boundaries (Emrath and Ford, 2016) to generate a low, medium, and high urban density scheme (Table 1 and 2).

Each of the six land uses were characterized with 30 9-acre sampling sites of uniform coverage (i.e. the alfalfa layer is comprised of just alfalfa sample sites of uniform coverage). Sample locations were randomly selected within each land cover type using a random point generator. All sample sets were used to calculate the seasonality and magnitude of ET for each land cover type.

We calculated the future irrigation water demand for the Treasure Valley using the calculated ET and a population growth model (Sprague et al., 2017). The model assumes a basin population of 1.5 million people by 2100, but three scenarios represent different rates of urban expansion, agricultural loss, and population density (Table 2). The “Business as Usual” scenario projects the current growth and expansion rate. The “Decreased Density” scenario assumes a large increase in the rate of urban expansion and agricultural conversion while the “Increased Density” scenario assumes a reduced rate of urban expansion and agricultural conversion.

The ET assigned to the modeled urbanized land is derived from the ET values calculated from the various land use samples, while the agricultural land maintained the current mean rate. The “Business as Usual” scenario used ET values from the current urban average. The “Decreased Density” scenario used ET values from the low-density

urban sample ET rate. The “Increased Density” scenario used ET values from the high-density urban sample ET rate. However, all projected values are estimates using current climate conditions and assume no large variations from currently modeled ET rates. Each projection also assumes all future developed land is strictly low, medium, or high density, respective of the calculated scenario. For example, the Increased Density scenario assumes all future urban development represents high-density ET values.

RESULTS

There was a strong relationship between the modeled and observed ET (adjusted r^2 0.85 at Boise and 0.79 at Parma) and the residuals were normally distributed (Figures 6 and 7). The data was split into a validation set consisting of 90% training and 10% test data. The test data had an adjusted r^2 value of 0.83 at Boise AgriMet and 0.77 at Parma.

The seasonal ET characteristics of agricultural and urban landscapes differed in both magnitude and timing. The total irrigation season ET per acre for the total urban land is 20% less than the total agricultural land (Figure 8). Total urban and agricultural land also feature a minor overlap of their 95% confidence interval (CI) ranges but fails to establish a true statistically significant relationship (Knezevic, 2008; Cumming, 2009). The total agricultural area had a higher daily average ET at 2.7 mm day^{-1}, producing a total seasonal average of 1.83 feet per acre. The total urban area averaged 2.2 mm day^{-1} and produced an average of 1.45 feet per acre over the irrigation season (Figure 8).

The alfalfa sample set had the highest total seasonal ET with 3.1 feet per acre over the irrigation season. The timing of the alfalfa crops shows a steady and gradual increase in ET from early April to mid-July where the daily consumption peaks, following the seasonality of temperature (Figure 9). The total modeled ET and its seasonal pattern is consistent with previous studies in nearby Kimberly, ID which calculated alfalfa ET to be approximately 3 feet a season on average (Shewmaker, Allen, and Neibling, 2011).

The corn sample set had a total seasonal ET of 2.3 feet per acre. The seasonality and total ET are close to estimates of late season corn of approximately 2.1 feet per acre

in a similar climate (Allen and Robison, 2017). The seasonality of ET for this crop type reflects very low average ET until mid-July where ET climbs and peaks rapidly which is also aligned with temperature trends (Figure 9).

The wheat sample set had a total seasonal ET of 2.1 feet per acre. The total ET per acre is slightly lower than the estimate from Allen and Robison (2017) of approximately 2.5 feet per acre. The seasonality of ET from wheat shows a faster rate of increasing daily ET when compared to corn and is more in line with alfalfa. From its early intensity peak in July, the daily ET is minimal until the end of the season (Figure 9). The seasonality of wheat ET matches the wheat trend of previous studies in a similar climate (Allen and Robison, 2017).

ET Projections Under Urbanization Scenarios

All three urban density sample sets show seasonal patterns in ET that are very similar to the alfalfa samples and temperature patterns (Figure 10,11), but with lower average ET. The low-density sample set showed the highest total seasonal ET at 2.6 feet per acre, followed by the medium-density set at 2.1 feet per acre, and the high-density sample set at 1.7 feet per acre (Figure 12).

Under the “Business as Usual” scenario, the basin will see an increase of 29% in irrigation water demand by 2100 (Table 3). This scenario assumes current urban expansion and housing density rates don’t change from current conditions. This scenario results in a 160% increase in total urban land area and a 50% conversion of current agricultural land to urban land (Table 2).

The “Decreased Density” growth model projects 52% increased irrigation water demand by 2100 (Table 3). This scenario features a high rate of urban expansion and

decreased housing density. This results in an increase of current urban land by 180% and a conversion of 60% of agricultural land (Table 2).

The “Increased Density” growth model projects 2% increased irrigation water demand by 2100 (Table 3). This scenario features the lowest rate of urban expansion and highest rate of population density. The total urban area increases by 96% and a conversion of 31% of current agricultural land (Table 2).

DISCUSSION

Understanding ET and its effect on the local water balance is essential in semiarid regions susceptible to annual water stress due to limited water availability. Continued urbanization in these areas further complicates the local water balance by altering the current landscape ET rate and historic water demand. Tracking and measuring the change in water demand through ET alone is difficult, but there are new methods that provide greatly improved temporal and spatial ET estimates. Here, we applied a common remote sensing ET method to a higher temporally and spatially resolved set of imagery to assess how the difference in ET between urban and agricultural land covers. The modeled ET data was used to estimate the potential effects of various growth scenarios on irrigation water demand in a semiarid metropolitan area.

We found that the seasonal difference in ET between agricultural and urban land uses within the Lower Boise River Basin is relatively small, despite large variation in their respective daily ET. While the agricultural area features a higher average ET per acre, the seasonal variability is a function of plant phenology. In contrast, the urban area has a lower average ET per acre but is more consistent through the irrigation season. (Figure 11). Although the urban area might have lower ET on average, the high resolution of the ET estimates allowed for analysis of various densities of urban development and impact of vegetation phenology. Urban land may actually produce more ET per acre than adjacent agricultural lands because of the irrigated lawns and parks in low and medium density suburbs. For example, the low-density urban sample set was

shown to consume more water per acre than both the corn and wheat samples sets (Figure 12).

The overall average consumptive similarities between the agricultural and urban areas appear to be a function of not just the total ET but in large part by vegetation phenology. While farm crops feature a higher peak ET intensity, they also undergo different stages of growth and harvesting, resulting in large fluctuations in ET rates through time (Figure 11). This was especially evident in analyzing the corn and wheat crop samples. Both crop types exhibit high ET during one half of the season, but then have a very low ET rate during the other half. The urban areas, which typically feature a sparser vegetation coverage, has a moderate ET that is lower than in the agricultural areas, but it is consistent for a longer period.

As urbanization continues, we will need to assess how much more water is needed to support irrigation demands in the basin. The shift in irrigation will be dependent on what type of land is being converted (agricultural or currently undeveloped) and associated vegetation type. When land is converted from agriculture to urban, there will be minimal changes in net ET because both land uses currently use water for irrigation. Converting undeveloped land, however, will have significant impacts on lower basin water use because these landscapes do not currently have any commercial or residential uses. Urbanizing this undeveloped land will result in significant increases in total ET across the basin. The conversion of agriculture land to accommodate urban expansion rather than converting undeveloped land would thus have a smaller net increase on future water demand. The increase in irrigation water demand from urbanization will have

impacts on water resources, likely through increased dependence on municipal groundwater supply.

Although the high-resolution remote sensing data used in this study is highly valuable, direct measures of ET across the different land uses would provide a better validation data set. These instruments would also increase the accuracy and reliability of the ET modeling algorithm. Improving the modeling precision would add more reliability to future water demand predictions. A thorough landscape conversion analysis between agriculture, urban, and undeveloped land would provide a better estimate of future irrigation water demand estimates by better constraining the types of future developments.

Conclusion

Using newly available, high resolution imagery, we spatially modeled ET within the Lower Boise River Basin and found a small difference in the average ET per acre between the total agricultural and urban areas. However, examining specific land use samples show that some urban areas feature higher ET rates than some agricultural areas. The differences in the seasonality and total seasonal ET between urban and agricultural land is highly variable over a 204-day period and dependent on vegetation type and density (Figure 11). When combined with previous studies of population growth modeling, our ET estimates indicate a projected increase in future irrigation demand upwards of 50% by the year 2100. However, the true increase in irrigation demand is dependent on the future population density, urban expansion, land type conversion, climate change, and associated impacts on water supply and atmospheric water deficit. This study highlights that vegetation phenology and housing density in urban

environments is an important factor in assessing differences in ET between agricultural and urban environments.

Data Availability

ET Image Data available via Boise State Library

Code Repository: https://github.com/curtiscrandall/Thesis_Research

REFERENCES

Alfieri, J. G., Kustas, W. P., & Anderson, M. C. (2018). A Brief Overview of Approaches for Measuring Evapotranspiration. Agroclimatology: Linking Agriculture to Climate, (agronmonogr60).

Allen, R. G. (2000). Using the FAO-56 dual crop coefficient method over an irrigated region as part of an evapotranspiration intercomparison study. Journal of Hydrology, 229(1-2), 27-41.

Allen, R. G. (2002). Conversion of Wright (1981) and Wright (1982) alfalfa-based crop coefficients for use with the ASCE Standardized Penman-Monteith Reference Evapotranspiration Equation. Technical Note-USDA-ARS, Kimberly, Id.

Allen, Richard G. and Clarence W. Robison. (2017). Evapotranspiration and Consumptive Irrigation Water Requirements for Idaho: Supplement updating the Time Series through December 2017, Research Technical Completion Report, Kimberly Research and Extension Center, University of Idaho, Moscow, ID.

Allen, R. G., Clemmens, A. J., Burt, C. M., Solomon, K., & O'Halloran, T. (2005a). Prediction accuracy for project wide evapotranspiration using crop coefficients and reference evapotranspiration. Journal of Irrigation and Drainage Engineering, 131(1), 24-36.

Allen, R. G., Jensen, M. E., Wright, J. L., & Burman, R. D. (1989). Operational estimates of reference evapotranspiration. Agronomy journal, 81(4), 650-662.

Allen, R. G., Pereira, L. S., Smith, M., Raes, D., & Wright, J. L. (2005b). FAO-56 dual crop coefficient method for estimating evaporation from soil and application extensions. Journal of irrigation and drainage engineering, 131(1), 2-13.

Allen, R. G., Pereira, L. S., Raes, D., & Smith, M. (1998). Crop evapotranspiration-Guidelines for computing crop water requirements-FAO Irrigation and drainage paper 56. FAO, Rome, 300(9), D05109.

Allen, R. G., Pereira, L. S., Howell, T. A., & Jensen, M. E. (2011). Evapotranspiration information reporting: I. Factors governing measurement accuracy. Agricultural Water Management, 98(6), 899-920.

Allen, R. G., Tasumi, M., & Trezza, R. (2007). Satellite-based energy balance for mapping evapotranspiration with internalized calibration (METRIC)—Model. Journal of irrigation and drainage engineering, 133(4), 380-394.

Amatya, D. M., Skaggs, R. W., & Gregory, J. D. (1995). Comparison of methods for estimating REF-ET. Journal of irrigation and drainage engineering, 121(6), 427-435.

ASCE-EWRI. (2005). The ASCE standardized reference evapotranspiration equation. Technical Committee Rep. to the Environmental and Water Resources Institute of ASCE from the Task Committee on Standardization of Reference Evapotranspiration.

Barnett, T. P., Adam, J. C., & Lettenmaier, D. P. (2005). Potential impacts of a warming climate on water availability in snow-dominated regions. Nature, 438(7066), 303.

Cumming, G. (2009). Inference by eye: reading the overlap of independent confidence intervals. Statistics in medicine, 28(2), 205-220.

DiGiovanni-White, K., Montalto, F., & Gaffin, S. (2018). A comparative analysis of micrometeorological determinants of evapotranspiration rates within a heterogeneous urban environment. Journal of hydrology, 562, 223-243.

Ehrlich, P. R., & Ehrlich, A. H. (1990). The population explosion.

Emrath, P., & Ford, C. (2016). Typical American subdivisions. National Association of Home Builders (NAHB). 3 Oct.

Gavilan, P., Berengena, J., & Allen, R. G. (2007). Measuring versus estimating net radiation and soil heat flux: impact on Penman–Monteith reference ET estimates in semiarid regions. Agricultural Water Management, 89(3), 275-286.

Geospatial Technology Section, Idaho Department of Water Resources. (2015). Irrigated Lands for the Treasure Valley (TV). Idaho Department of Water Resources. http:/idwr.idaho.gov, https://idwr.idaho.gov/gis.

Glenn, E. P., Nagler, P. L., & Huete, A. R. (2010). Vegetation index methods for estimating evapotranspiration by remote sensing. Surveys in Geophysics, 31(6), 531-555.

Grimmond, C. S. B., & Oke, T. R. (1999). Aerodynamic properties of urban areas derived from analysis of surface form. Journal of applied meteorology, 38(9), 1262-1292.

Henggeler, J. C., Guinan, P., & Travlos, J. (2008, November). Procedure to easily Fine-Tune Crop Coefficients for Irrigation Scheduling. In Proc. of 2008 International Irrigation Technical Conference Conf (pp. 2-4).

Howell, T. A., Schneider, A. D., & Jensen, M. E. (1991, July). History of lysimeter design and use for evapotranspiration measurements. In Lysimeters for evapotranspiration and environmental measurements (pp. 1-9). ASCE.

Itenfisu, D., Elliott, R. L., Allen, R. G., & Walter, I. A. (2003). Comparison of reference evapotranspiration calculations as part of the ASCE standardization effort. Journal of Irrigation and Drainage Engineering, 129(6), 440-448.

Kamble, B., Kilic, A., & Hubbard, K. (2013). Estimating crop coefficients using remote sensing-based vegetation index. Remote sensing, 5(4), 1588-1602.

Khoob, A. R. (2008). Comparative study of Hargreaves's and artificial neural network's methodologies in estimating reference evapotranspiration in a semiarid environment. Irrigation Science, 26(3), 253-259.

Kite, G. W., & Droogers, P. (2000). Comparing evapotranspiration estimates from satellites, hydrological models and field data. Journal of Hydrology, 229(1-2), 3-18.

Knezevic, A. (2008). Overlapping confidence intervals and statistical significance. StatNews: Cornell University Statistical Consulting Unit, 73(1).

López-Urrea, R., de Santa Olalla, F. M., Fabeiro, C., & Moratalla, A. (2006). Testing evapotranspiration equations using lysimeter observations in a semiarid climate. Agricultural water management, 85(1-2), 15-26.

Miles, J. (2005). R-Squared, Adjusted R-Squared. Encyclopedia of Statistics in Behavioral Science.

Montgomery, D. C., Peck, E. A., & Vining, G. G. (2012). Introduction to linear regression analysis (Vol. 821). John Wiley & Sons.

Nagler, Pamela L., James Cleverly, Edward Glenn, Derrick Lampkin, Alfredo Huete, and Zhengming Wan. "Predicting riparian evapotranspiration from MODIS vegetation indices and meteorological data." Remote Sensing of Environment 94, no. 1 (2005): 17-30.

Nagler, P., Glenn, E., Nguyen, U., Scott, R., & Doody, T. (2013). Estimating riparian and agricultural actual evapotranspiration by reference evapotranspiration and MODIS enhanced vegetation index. Remote Sensing, 5(8), 3849-3871.

Niemczynowicz, J. (1999). Urban hydrology and water management–present and future challenges. Urban water, 1(1), 1-14.

Nouri, H., Beecham, S., Anderson, S., & Nagler, P. (2014). High spatial resolution WorldView-2 imagery for mapping NDVI and its relationship to temporal urban landscape evapotranspiration factors. Remote sensing, 6(1), 580-602.

Nouri, H., Glenn, E., Beecham, S., Chavoshi Boroujeni, S., Sutton, P., Alaghmand, S., ... & Nagler, P. (2016). Comparing three approaches of evapotranspiration estimation in mixed urban vegetation: field-based, remote sensing-based and observational-based methods. Remote Sensing, 8(6), 492.

Paço, T. A., Pôças, I., Cunha, M., Silvestre, J. C., Santos, F. L., Paredes, P., & Pereira, L. S. (2014). Evapotranspiration and crop coefficients for a super intensive olive orchard. An application of SIMDualKc and METRIC models using ground and satellite observations. Journal of hydrology, 519, 2067-2080.

Petrich, Christian. (2016). Treasure Valley DCMI Water-Demand Project (2015-2065). SPF Water Engineering, LLC; Idaho Water Resource Board; Idaho Department of Water Resources.

Qiu, G. Y., LI, H. Y., Zhang, Q. T., Wan, C. H. E. N., Liang, X. J., & Li, X. Z. (2013). Effects of evapotranspiration on mitigation of urban temperature by vegetation and urban agriculture. Journal of Integrative Agriculture, 12(8), 1307-1315.

Shewmaker, G. E., Allen, R. G., & Neibling, W. H. (2011). Alfalfa irrigation and drought. University of Idaho, College of Agricultural and Life Sciences: Moscow, ID, USA.

Sprague, C., Fragkias, M., Narducci, J., Brandt, J., & Benner, S. G. (2017). Raster Data for Projecting Urban Expansion in the Treasure Valley (Idaho) to Year 2100 Under Different Scenarios of Population Growth and Housing Density.

Stow, D., Coulter, L., Kaiser, J., Hope, A., Schutte, K., & Walters, A. (2003). Irrigated vegetation assessment for urban environments. Photogrammetric Engineering & Remote Sensing, 69(4), 381-390.

Taha, H. (1997). Urban climates and heat islands: albedo, evapotranspiration, and anthropogenic heat. Energy and buildings, 25(2), 99-103.

Templeton, N. P., Vivoni, E. R., Wang, Z. H., & Schreiner-McGraw, A. P. (2018). Quantifying water and energy fluxes over different urban land covers in Phoenix, Arizona. Journal of Geophysical Research: Atmospheres, 123(4), 2111-2128.

Thornton, P. E., Thornton, M. M., Mayer, B. W., Wilhelmi, N., Wei, Y., Devarakonda, R., & Cook, R. B. (2014). Daymet: Daily Surface Weather Data on a 1-km Grid for North America, Version 2. Oak Ridge National Lab.(ORNL), Oak Ridge, TN (United States).

Treasure Valley Water Atlas (Human-Environment Systems). (2018). The Narratives. Retrieved from https://www.boisestate.edu/hes/tvwa/narratives/

Trezza, R., Allen, R., & Tasumi, M. (2013). Estimation of actual evapotranspiration along the Middle Rio Grande of New Mexico using MODIS and Landsat imagery with the METRIC model. Remote Sensing, 5(10), 5397-5423.

USDA National Agricultural Statistics Service Cropland Data Layer. (2017). Published crop-specific data layer [Online]. Available at https://nassgeodata.gmu.edu/CropScape/ (accessed 2017; verified 2017). USDA-NASS, Washington, DC.

Valayamkunnath, P., Sridhar, V., Zhao, W., & Allen, R. G. (2018). Intercomparison of surface energy fluxes, soil moisture, and evapotranspiration from eddy covariance, large-aperture scintillometer, and modeling across three ecosystems in a semiarid climate. Agricultural and Forest Meteorology, 248, 22-47.

APPENDIX

Sentinel Image Processing

The Level-2A processing includes a scene classification and an atmospheric correction applied to Top-Of-Atmosphere (TOA) Level-1C orthoimage products. Level-2A main output is an orthoimage Bottom-Of-Atmosphere (BOA) corrected reflectance product.

Additional outputs are an Aerosol Optical Thickness (AOT) map, a Water Vapor (WV) map and a Scene Classification Map (SCM) together with Quality Indicators (QI) for cloud and snow probabilities at 60 m resolution. Level-2A output image products will be resampled and generated with an equal spatial resolution for all bands (10 m, 20 m or 60 m). Standard distributed products contain the envelope of all resolutions in three distinct folders:

- 10 m: containing spectral bands 2, 3, 4, 8, a True Color Image (TCI) and an AOT and WV maps resampled from 20 m.
- 20 m: containing spectral bands 2 - 7, the bands 8A, 11 and 12, a True Color Image (TCI), a Scene Classification map (SCL) and an AOT and WV map. The band B8 is omitted as B8A provides more precise spectral information.
- 60 m: containing all components of the 20 m product resampled to 60 m and additionally the bands 1 and 9. The cirrus band 10 is omitted, as it does not contain surface information.

The Sen2Cor [R1] processor algorithm is a combination of state-of-the-art techniques for performing atmospheric corrections which have been tailored to the Sentinel-2 environment together with a scene classification module described in [R2]. The scene classification algorithm allows detection of clouds, snow and cloud shadows and generation of a classification map, which consists of three different classes for clouds

(including cirrus), together with six different classifications for shadows, cloud shadows, vegetation, not vegetated, water and snow.

The algorithm is based on a series of threshold tests that use as input TOA reflectance as input from the Sentinel-2 spectral bands. In addition, thresholds are applied on band ratios and indexes like Normalized Difference Vegetation Index (NDVI) and Normalized Difference Snow and Ice Index (NDSI). For each of these threshold tests, a level of confidence is associated. It produces at the end of the processing chain a probabilistic cloud mask quality indicator and a snow mask quality indicator. The algorithm uses the reflective properties of scene features to establish the presence or absence of clouds in a scene. Cloud screening is applied to the data to retrieve accurate atmospheric and surface parameters, either as input for the further processing steps below or for being valuable input for processing steps of higher levels.

The aerosol type and visibility or optical thickness of the atmosphere is derived using the Dense Dark Vegetation (DDV) algorithm [R3]. This algorithm requires that the scene contains reference areas of known reflectance behavior, preferably DDV and water bodies. The algorithm starts with a user-defined visibility (default: 40 km). If the scene contains no dark vegetation or soil pixels, the surface reflectance threshold in the 2 190 nm band is successively iterated to include medium brightness reference pixels. If the scene contains no reference and no water pixels the scene is processed with the start visibility instead.

Water vapor retrieval over land is performed with the Atmospheric Pre-corrected Differential Absorption (APDA) algorithm [R4] which is applied to the two Sentinel-2 bands (B8a, and B9). Band 8a is the reference channel in an atmospheric window region.

Band 9 is the measurement channel in the absorption region. The absorption depth is evaluated in the way that the radiance is calculated for an atmosphere with no water vapor assuming that the surface reflectance for the measurement channel is the same as for the reference channel. The absorption depth is then a measure of the water vapor column content.

Atmospheric correction is performed using a set of look-up tables generated via libRadtran. Baseline processing is the rural/continental aerosol type. Other look-up tables can also be used according to the scene geographic location and climatology.

[R1]: M. Main-Knorn, B. Pflug, J. Louis, V. Debaecker, U. Müller-Wilm, F. Gascon, "Sen2Cor for Sentinel-2", Proc. SPIE 10427, Image and Signal Processing for Remote Sensing XXIII, 1042704 (2017)

[R2]: J. Louis, A. Charantonis & B. Berthelot, "Cloud Detection for Sentinel-2", Proceedings of ESA Living Planet Symposium (2010)

[R3]: Kaufman, Y., Sendra, C. Algorithm for automatic atmospheric corrections to visible and near-IR satellite imagery, International Journal of Remote Sensing, Volume 9, Issue 8, 1357-1381 (1988)

[R4]: Schläpfer, D. et al., "Atmospheric precorrected differential absorption technique to retrieve columnar water vapor", Remote Sens. Environ., Vol. 65, 353366 (1998)

Reference ET

In 1948, Penman combined the energy balance with the mass transfer method and derived an equation to compute the evaporation from an open water surface from standard climatological records of sunshine, temperature, humidity and wind speed. This

so-called combination method was further developed by many researchers and extended to cropped surfaces by introducing resistance factors. The Penman-Monteith form of the combination equation is:

$$\lambda ET = \frac{\Delta(R_n - G) + (\text{pa} \cdot cp) + \frac{(e_s - e_a)}{ra}}{\Delta + \gamma(\frac{rs}{ra})}$$

where Rn is the net radiation, G is the soil heat flux, (es - ea) represents the vapor pressure deficit of the air, ra is the mean air density at constant pressure, cp is the specific heat of the air, Delta represents the slope of the saturation vapor pressure temperature relationship, gamma is the psychrometric constant, and rs and ra are the (bulk) surface and aerodynamic resistances.

The Penman-Monteith approach as formulated above includes all parameters that govern energy exchange and corresponding latent heat flux (evapotranspiration) from uniform expanses of vegetation. Most of the parameters are measured or can be readily calculated from weather data. The equation can be utilized for the direct calculation of any crop evapotranspiration as the surface and aerodynamic resistances are crop specific.

List of Figures

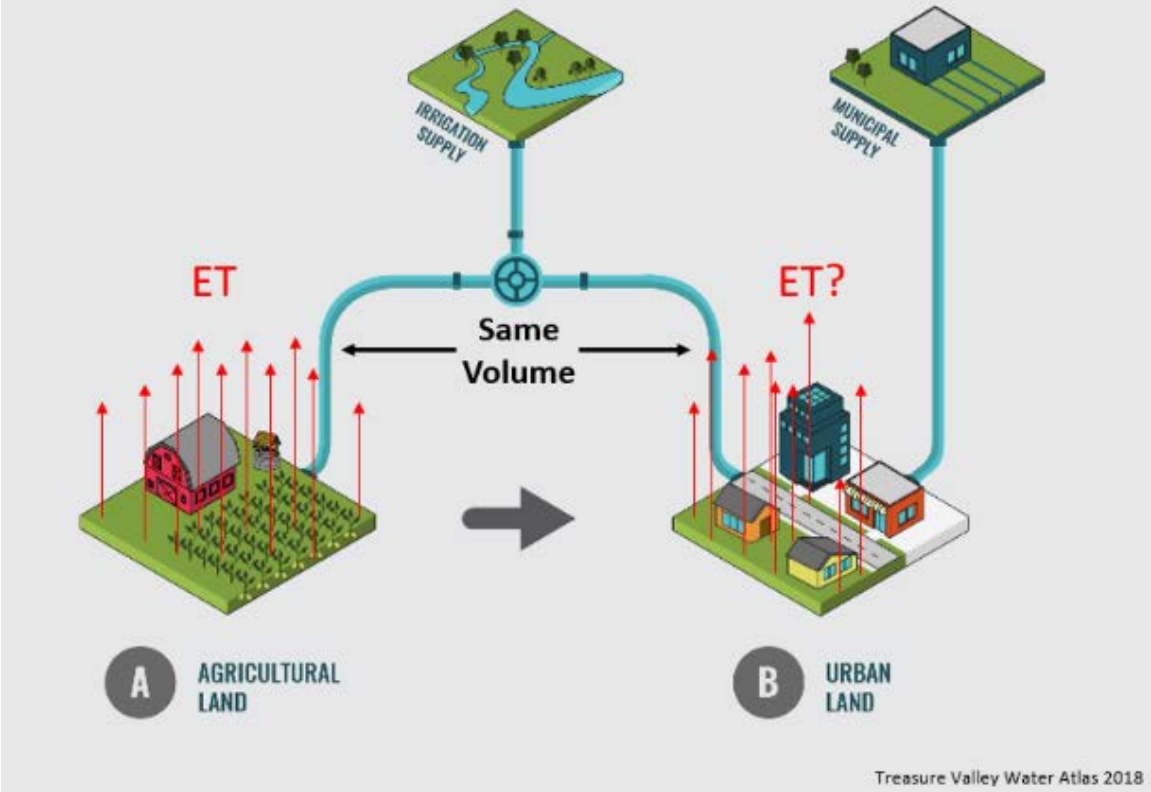

Figure 1. Above are examples of water supply and ET of agricultural and urban landscapes. Each landscape receives the same amount of irrigation water (assuming both utilize water rights), as water rights within the study area are based on land size. The urban landscape also typically receives an additional supply of municipal water for mainly indoor water use.

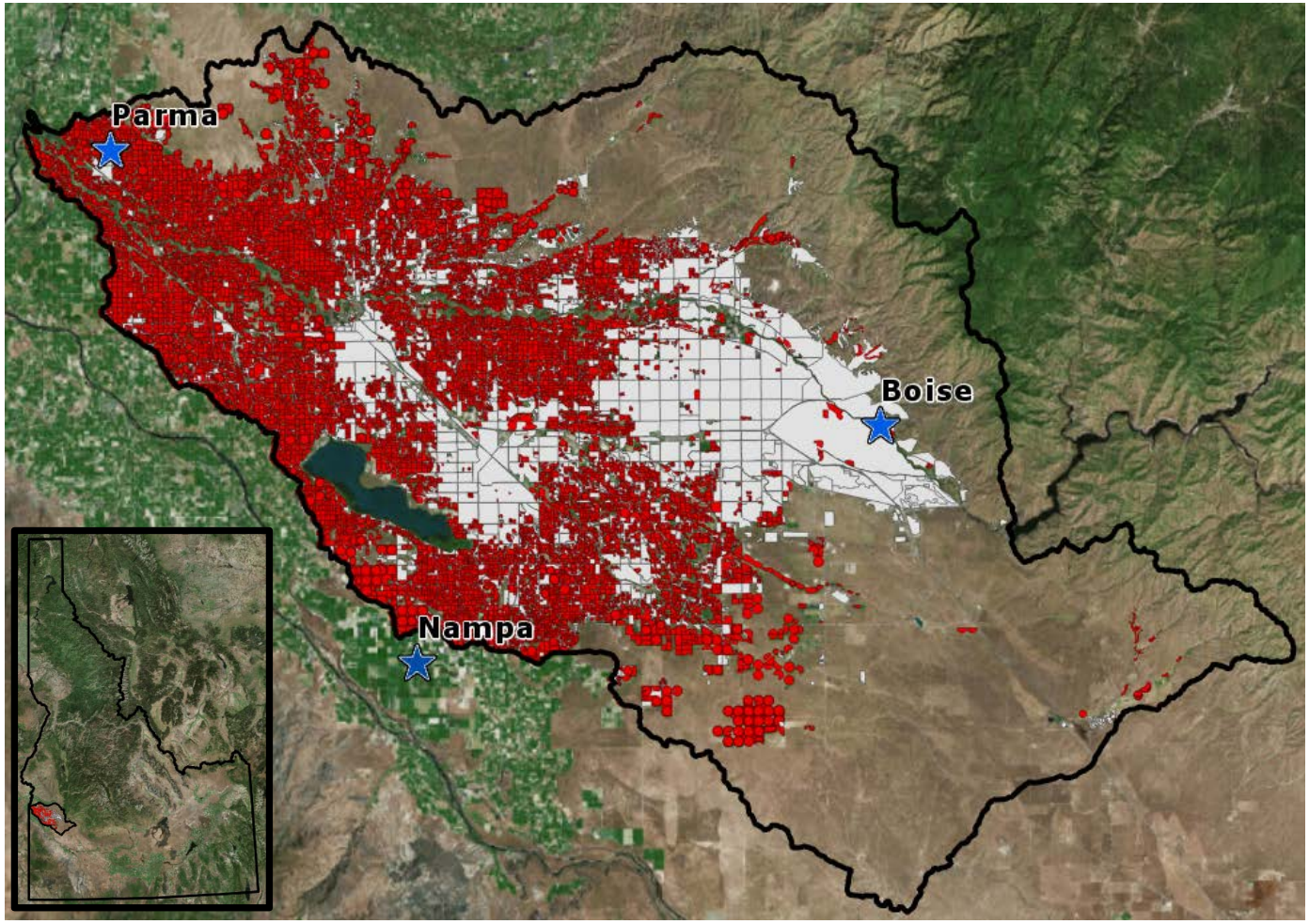

Figure 2. Above shows the 2015 IDWR land designation map and locations of the AgriMet stations (blue stars). 220,000 acres of agricultural area (irrigated land) is shown in red, and the 160,000 acres of urban area are colored grey. The Lower Boise River Basin NHD boundary is outlined in black.

Figure 3. Above shows the mass water balance of the Lower Boise River Basin. The graphic and data come from Boise State University's Treasure Valley Water Atlas.

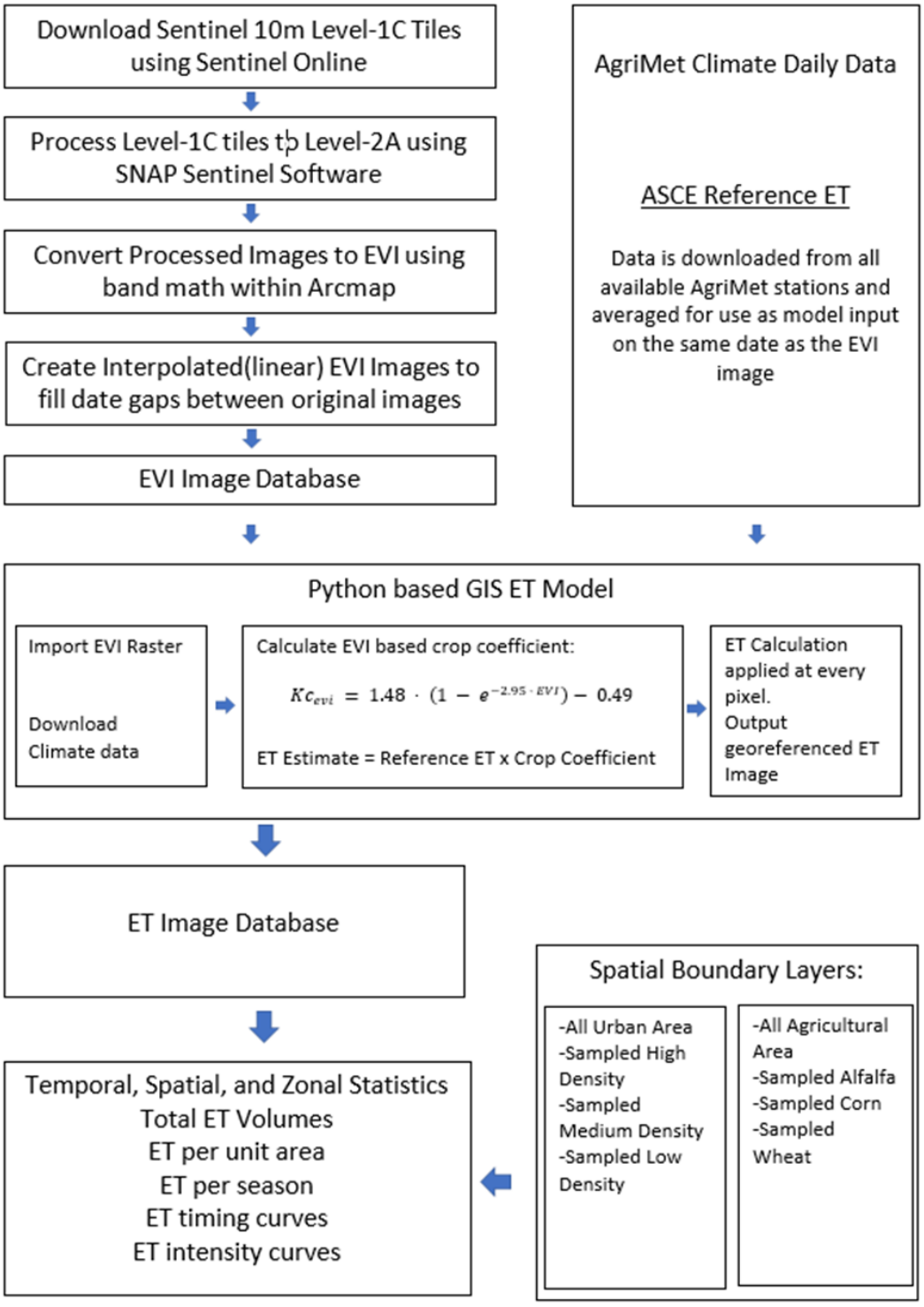

Figure 4. Above is the processing workflow of methods for this study.

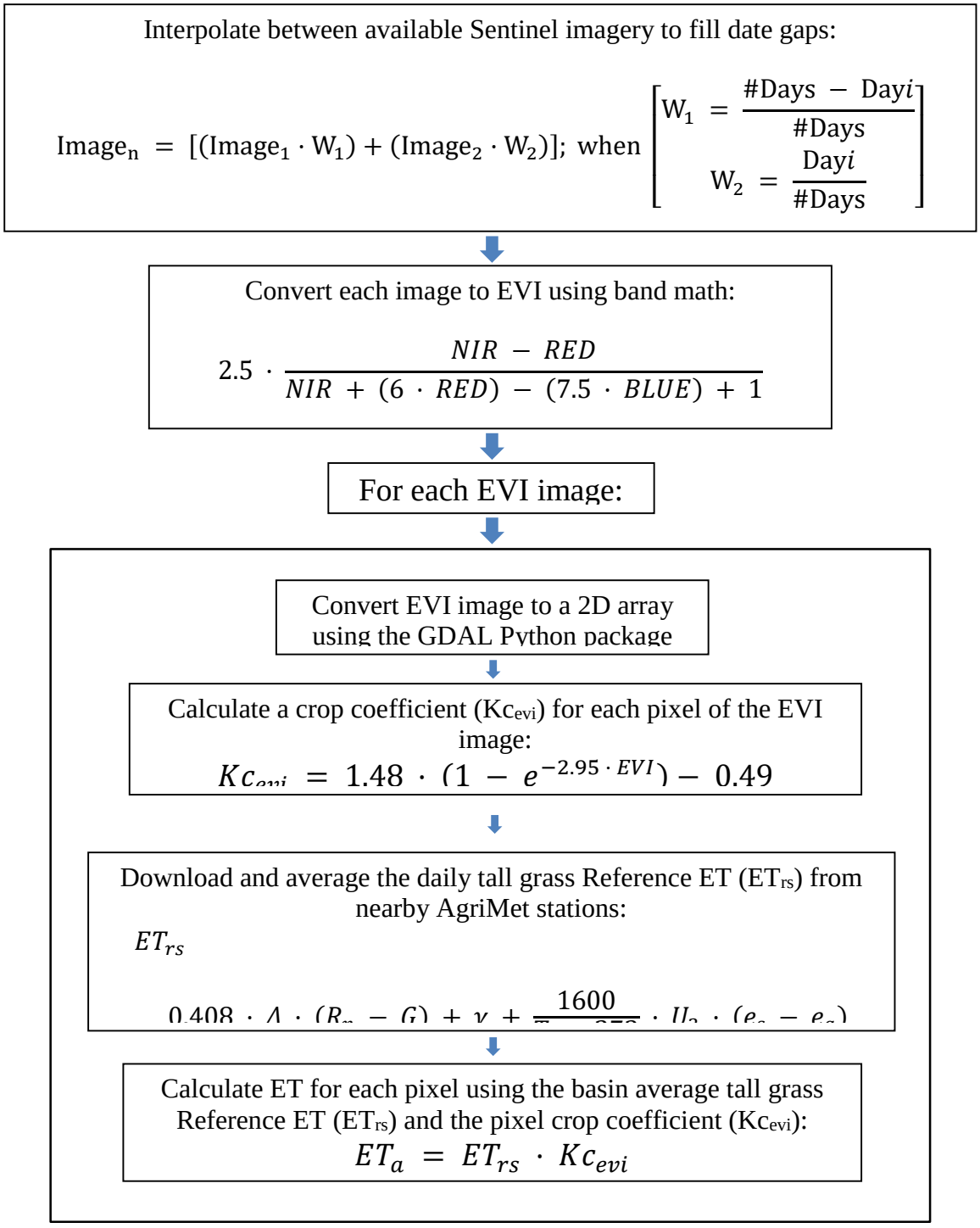

Figure 5. Above is the logic and equations from the model used to generate the ET data.

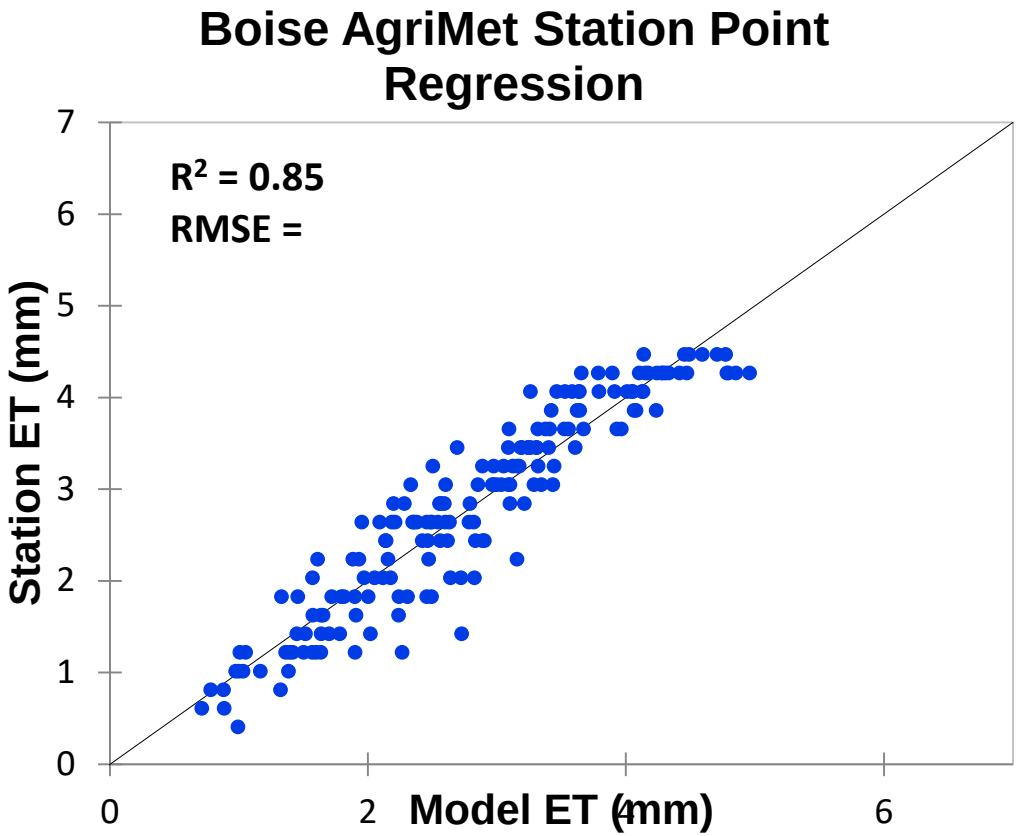

Figure 6. Above is the resulting linear regression analysis and fit of actual ET pixel values at the Boise AgriMet climate station location. The station values are the calculated actual ET at the station using a local crop coefficient table. The model values are the modeled actual ET using an EVI derived crop coefficient.

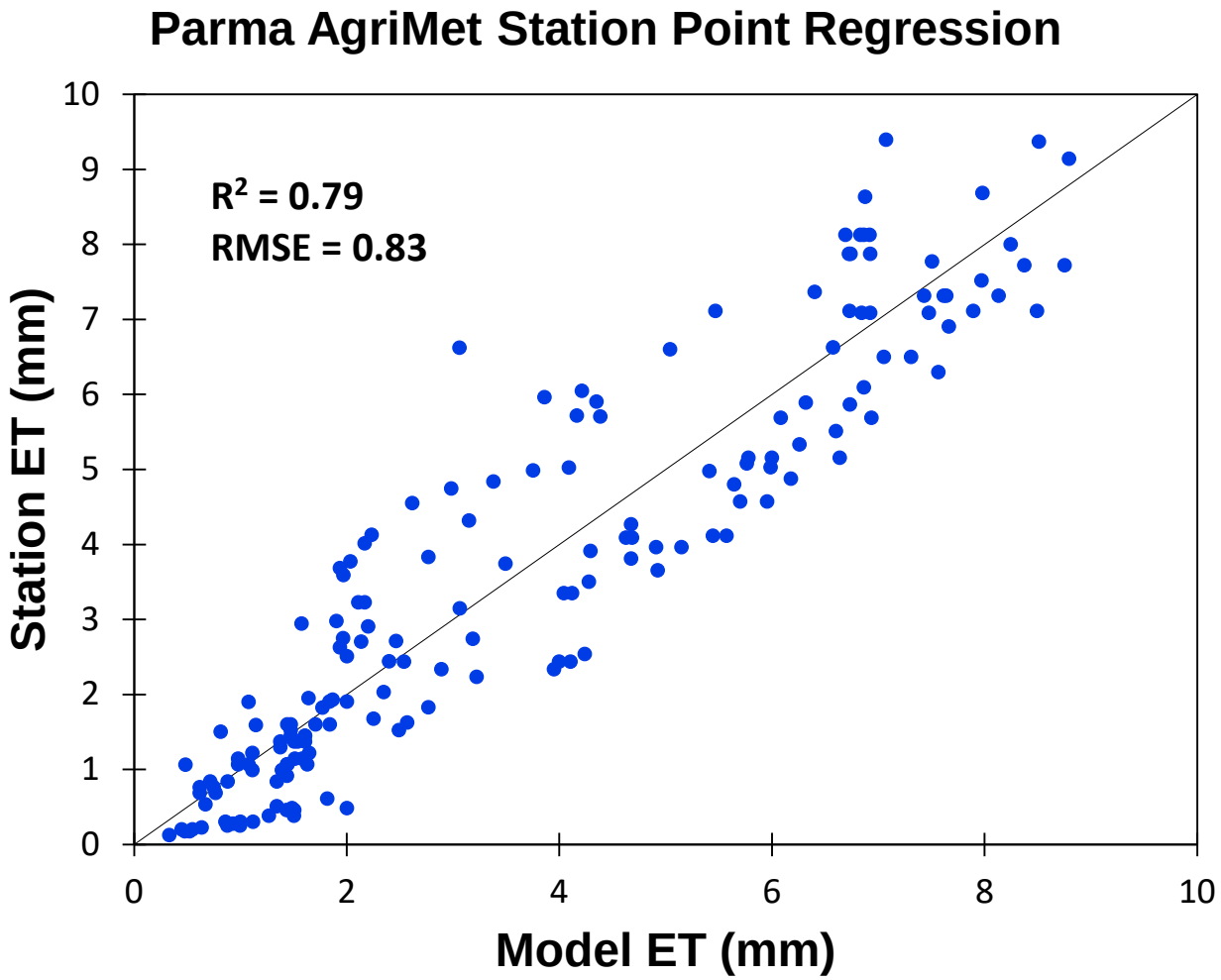

Figure 7. Above is the resulting linear regression analysis and fit of actual ET pixel values at the Parma AgriMet climate station location. The station values are the calculated actual ET at the station using a local crop coefficient table. The model values are the modeled actual ET using an EVI derived crop coefficient.

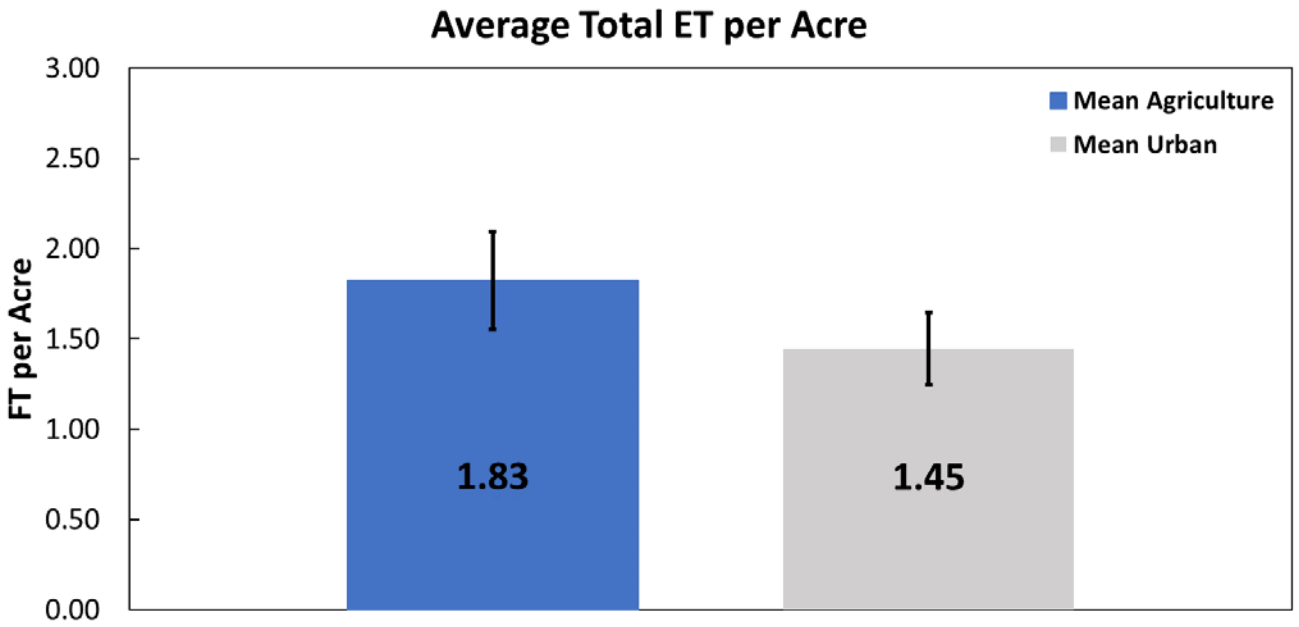

Figure 8. Shows the urban (as grey bar) and agricultural (as blue bar) area's total average landscape consumption (ET) in units of feet per acre. These values were calculated using the daily average ET divided by the daily acreage of active vegetation (EVI values greater than 0). The error bars indicate the 95% confidence interval of the 204-day population.

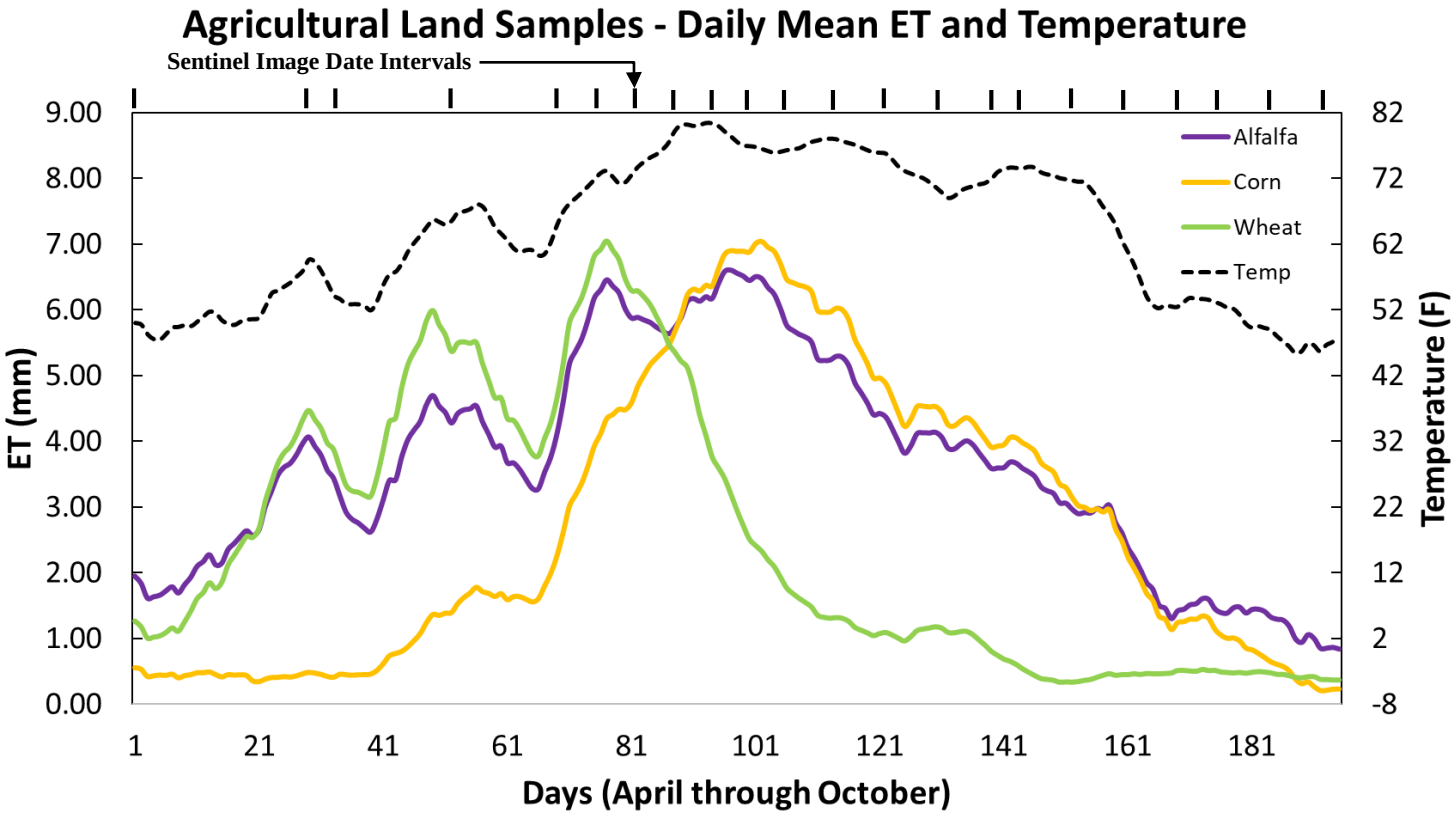

Figure 9. **Above shows the values and timing of the daily average temperatures across the Boise River Basin (as the black dashed line) along with the daily average ET values of the 3 different agricultural land samples (Alfalfa as the purple line, Corn as the gold line, Wheat as the green line).**

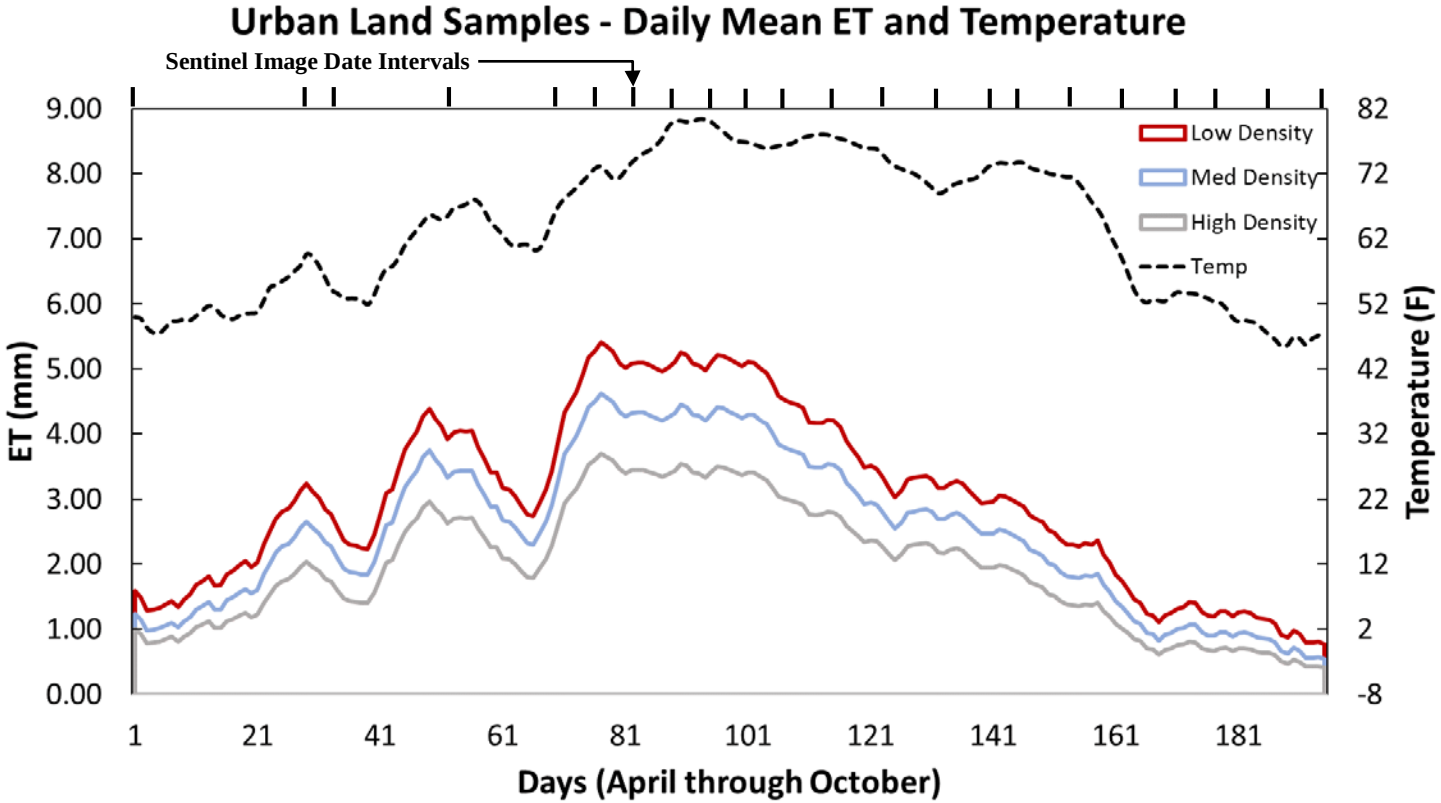

Figure 10. **Above shows the values and timing of the daily average temperatures across the Boise River Basin (as the black dashed line) along with the daily average ET values of the 3 different urban land samples (Low Density Urban as the red line, Medium Density Urban as the blue line, and High Density Urban as the grey line).**

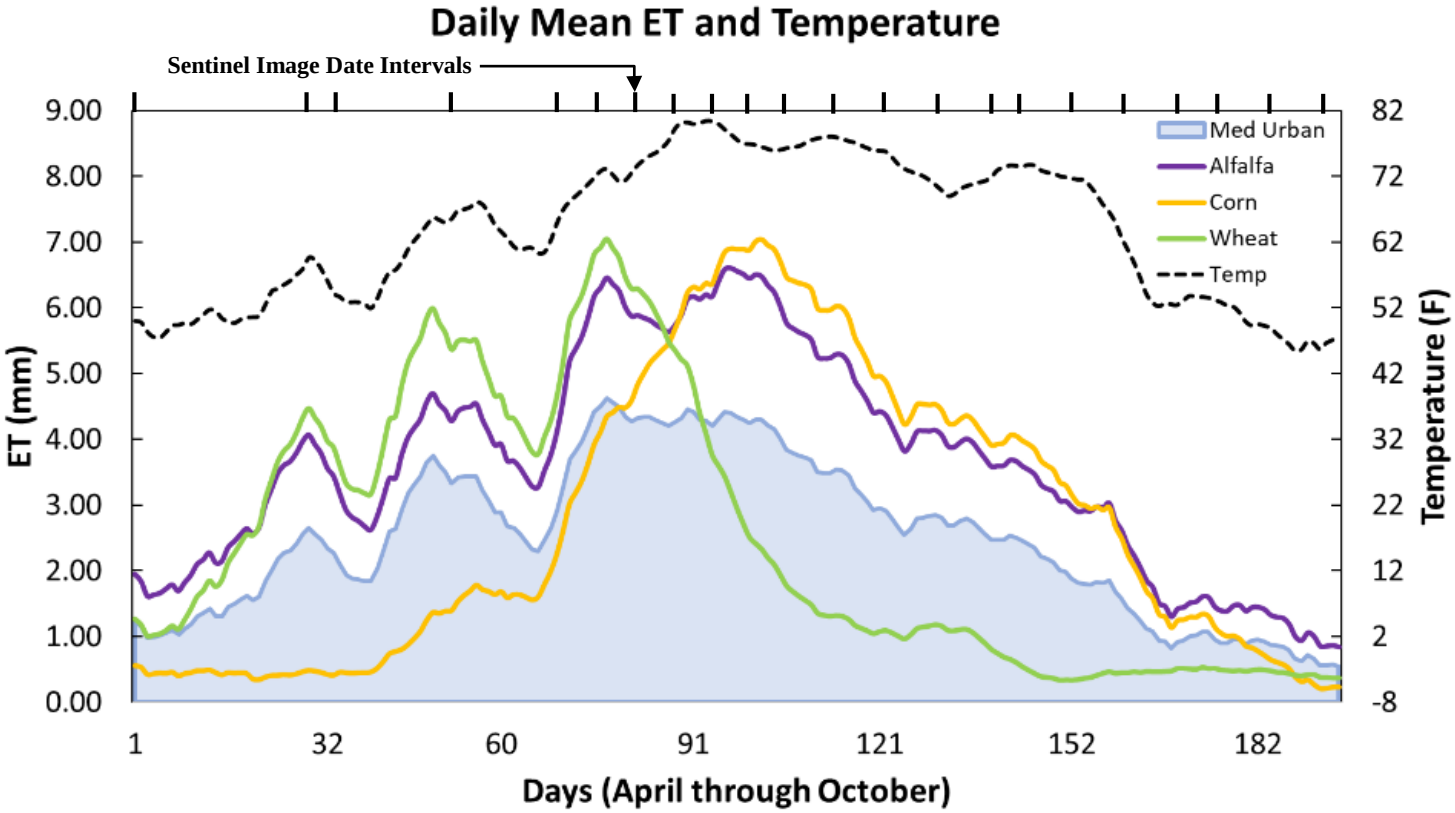

Figure 11. Above shows the values and timing of the daily average temperatures across the Boise River Basin (as the black dashed line) along with the daily average ET values of the 3 different agricultural land samples (Alfalfa as the purple line, Corn as the gold line, Wheat as the green line) and the average urban land sample (as the blue shaded region).

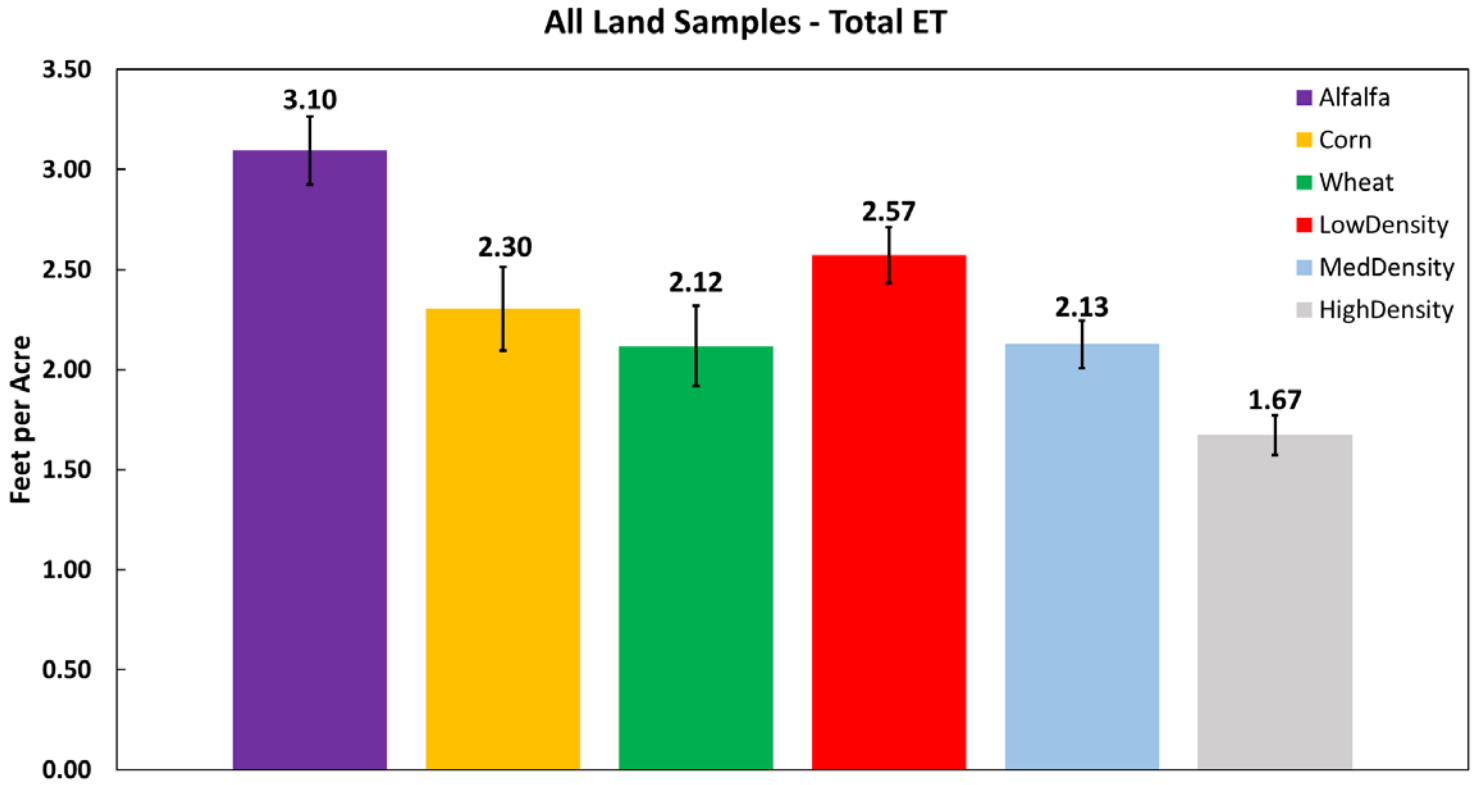

Figure 12. Above shows the average total consumption (ET) for each land type sample as feet per acre. From left to right, the purple bar represents Alfalfa, gold as Corn, green as Wheat, red as Low Density Urban, blue as Medium Density Urban, and grey as High Density Urban. Error is represented the 95% confidence interval for each sample of the 204-day population.

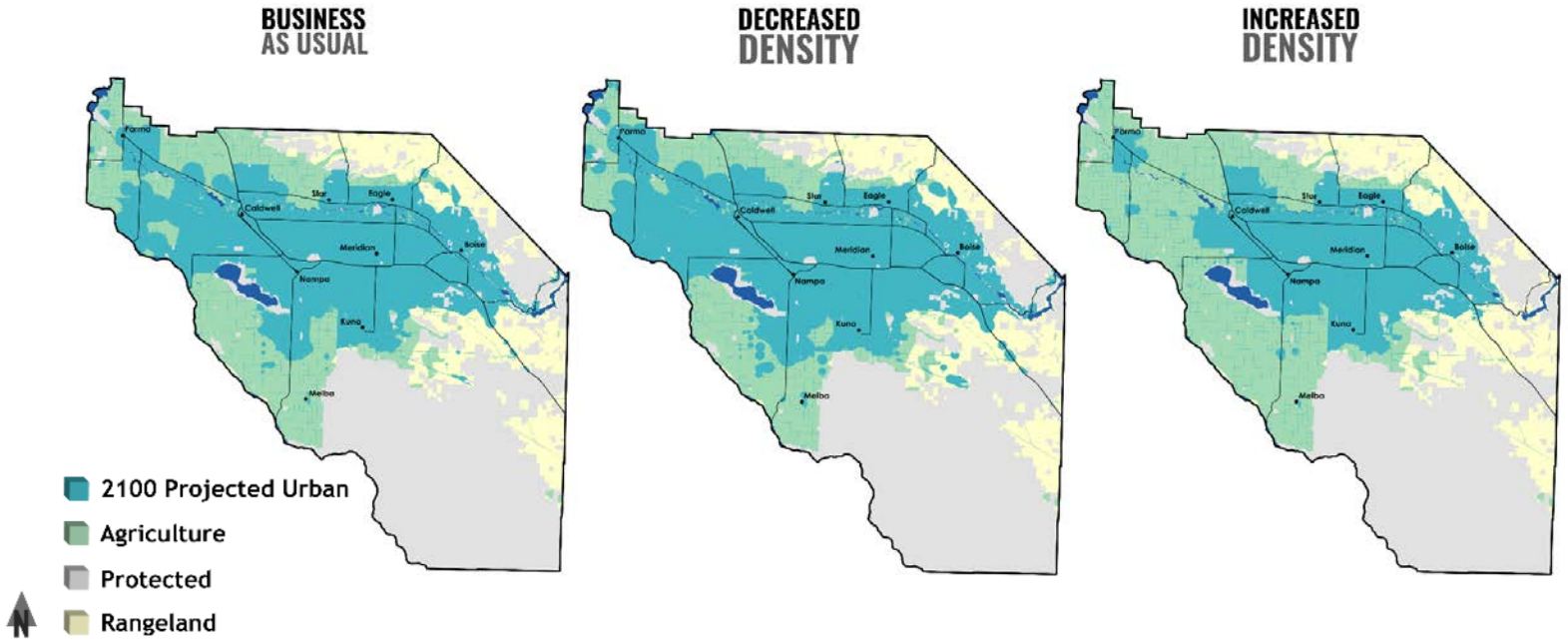

Figure 13. Above shows three different population growth models of the Treasure Valley from Sprague et al. 2017. The "Business as Usual" model (left) shows the future urban expansion using the basin's current growth values. The "Decreased Density" model (middle) shows the future urban expansion with a decreased population density (less people per acre), and the "Increased Density" (right) model shows the future urban with increased population density (more people per acre).

List of Tables

Table 1. Land Sample Density Ranking[1]

	Low Density	Medium Density	High Density
Houses per Acre	3	3.5	4
Houses per Land Sample Site	>10 and <21	>20 and <41	<61 and >40
People per Acre	8.1	9.5	10.8
People per Land Sample Site	25-55	55-110	110-165

1, The approximate density housing range was guided from the single-family metropolitan housing data according to the National Association of Home Builders. The U.S. Census Bureau statistics for the study area located in Idaho suggest an average 2.63 people per household. Each land sample set is a square 9-acre area.

Table 2. Projected Land Use Impact[1]

Scenario	Urban Gain (acres)	Agricultural Loss (acres)	Population in 2100	Population Density
Business as Usual	220,000	-190,000	1.5 million	4.14 people/acre
Low Population Density	260,000	-220,000	1.5 million	3.78 people/acre
High Population Density	140,000	-110,000	1.5 million	5.41 people/acre

1, the Sprague et al. 2017 comparison of urban expansion impacts on land use following different scenarios of increased population and variation in population density (variable urban expansion).

Table 3. Lower Boise River Basin Water Consumption Projections[1]

Land Type	Growth	Population	Area (acres)	Mean ET (feet per acre)	Urbanized Land ET (feet per acre)	Total ET (acre-ft)	Basin ET (acre-ft)
Current Lower Boise River Basin Data							
Urban	0	700k	160k	1.45	1.45	230k	630k
Agriculture	0		220k	1.83	1.45	400k	
2100 "Business as Usual" Projection							
Urban	160%	1,500k	420k	1.45	1.45	610k	810k
Agriculture	-52%		110k	1.83	1.83	200k	
2100 "Low Density" Projection							
Urban	180%	1,500k	450k	1.45	1.95	800k	960k
Agriculture	-60%		90k	1.83	1.83	160k	
2100 "High Density" Projection							
Urban	96%	1,500k	310k	1.45	0.95	370k	640k
Agriculture	-31%		150k	1.83	1.83	270k	

1, the current and projected landscape acreage and associated consumption values (ET) through the same 204-day irrigation season used in this study. The growth values come from the model projections shown in Sprague et al. 2017. The ET differences are calculated using the percent difference between high/low density urban sample data from this study (i.e. low-density urban is 35% more consumptive than high density urban (Figure 12)). The growth ET is calculated using 35% increase/decrease from current mean basin values depending on the density of projected urban expansion (Figure 8).